Influence of Connectivity and Porosity on Ligand-Based Luminescence in Zinc Metal−Organic Frameworks

Christina A. Bauer,[†] Tatiana V. Timofeeva,[§] Thomas B. Settersten,[||]
Brian D. Patterson,[||] Vincent H. Liu,[†] Blake A. Simmons,[†] and Mark D. Allendorf*,[‡]

*Contribution from the Department of Nanoscale Science and Technology, Department of
Microfluidics, and Combustion Research Facility, Sandia National Laboratories, Livermore,
California 94551, and Department of Natural Sciences, New Mexico Highlands University,
Las Vegas, New Mexico 87701*

Received January 3, 2007; E-mail: mdallen@sandia.gov

Abstract: Applications of metal−organic frameworks (MOFs) require close correlation between their structure and function. We describe the preparation and characterization of two zinc MOFs based on a flexible and emissive linker molecule, stilbene, which retains its luminescence within these solid materials. Reaction of *trans*-4,4′-stilbene dicarboxylic acid and zinc nitrate in *N,N*-dimethylformamide (DMF) yielded a dense 2-D network, **1**, featuring zinc in both octahedral and tetrahedral coordination environments connected by *trans*-stilbene links. Similar reaction in *N,N*-diethylformamide (DEF) at higher temperatures resulted in a porous, 3-D framework structure, **2**. This framework consists of two interpenetrating cubic lattices, each featuring basic zinc carboxylate vertices joined by *trans*-stilbene, analogous to the isoreticular MOF (IRMOF) series. We demonstrate that the optical properties of both **1** and **2** correlate with the local ligand environments observed in the crystal structures. Steady-state and time-resolved spectroscopic measurements reveal that the stilbene linkers in the dense structure **1** exhibit a small degree of interchromophore coupling. In contrast, the stilbenoid units in **2** display very little interaction in this low-density 3-D framework, with excitation and emission spectra characteristic of monomeric stilbenes, similar to the dicarboxylic acid in dilute solution. In both cases, the rigidity of the stilbene linker increases upon coordination to the inorganic units through inhibition of torsion about the central ethylene bond, resulting in luminescent crystals with increased emission lifetimes compared to solutions of *trans*-stilbene. The emission spectrum of **2** is found to depend on the nature of the incorporated solvent molecules, suggesting use of this or related materials in sensor applications.

Introduction

Understanding and predicting the photophysical properties of chromophores in the solid state is important for an increasing number of organic materials applications, where control over the spatial interactions of chromophores represents a significant challenge.[1−3] The geometry of a molecular assembly is often difficult to predict due to the large number of intermolecular forces that can influence the packing of molecules in a crystal. Metal−organic frameworks (MOFs) are a class of crystalline coordination polymers with the potential to control these interactions through appropriate choice of the constituent metal and ligand units. MOFs consist of metal ions or clusters connected by organic linker groups, which can lead to structural

rigidity, high porosity, and well-defined architectures.[4−6] These properties are desirable for a variety of applications, and the use of MOFs for gas storage,[7,8] drug delivery,[9] separations,[10−12] and catalysis[13,14] is currently being explored. The structural stability of MOFs results from strong metal−ligand coordination, which can afford some degree of predictability to the framework geometry and leads toward rational methods of crystal engineering. This has been utilized as a strategy to engineer noncentrosymmetric crystals for nonlinear optics

[†] Nanoscale Science and Technology Department, Sandia National Laboratories.
[‡] Microfluidics Department, Sandia National Laboratories.
[||] Combustion Research Facility, Sandia National Laboratories.
[§] New Mexico Highlands University.

(1) Gierschner, J.; Mack, H. G.; Oelkrug, D.; Waldner, I.; Rau, H. *J. Phys. Chem. A* **2004**, *108*, 257−263.
(2) Bazan, G. C.; Oldham, W. J.; Lachicotte, R. J.; Tretiak, S.; Chernyak, V.; Mukamel, S. *J. Am. Chem. Soc.* **1998**, *120*, 9188−9204.
(3) Shukla, A. D.; Strawser, D.; Lucassen, A. C. B.; Freeman, D.; Cohen, H.; Jose, D. A.; Das, A.; Evmenenko, G.; Dutta, P.; van der Boom, M. E. *J. Phys. Chem. B* **2004**, *108*, 17505−17511.
(4) Rowsell, J. L. C.; Yaghi, O. M. *Micropor. Mesopor. Mater.* **2004**, *73*, 3−14.
(5) Janiak, C. *J. Chem. Soc., Dalton Trans.* **2003**, 2781−2804.
(6) Kitagawa, S.; Kitaura, R.; Noro, S. *Angew. Chem. Int. Ed.* **2004**, *43*, 2334−2375.
(7) Rowsell, J. L. C.; Yaghi, O. M. *J. Am. Chem. Soc.* **2006**, *128*, 1304−1315.
(8) Millward, A. R.; Yaghi, O. M. *J. Am. Chem. Soc.* **2005**, *127*, 17998−17999.
(9) Horcajada, P.; Serre, C.; Vallet-Regi, M.; Seban, M.; Taulelle, F.; Ferey, G. *Angew. Chem., Int. Ed.* **2006**, *45*, 5974−5978.
(10) Lee, E. Y.; Suh, M. P. *Angew. Chem., Int. Ed.* **2004**, *43*, 2798−2801.
(11) Kitaura, R.; Fujimoto, K.; Noro, S.-I.; Kondo, M.; Kitagawa, S. *Angew. Chem., Int. Ed.* **2002**, *41*, 133−135.
(12) Chen, B. L.; Liang, C. D.; Yang, J.; Contreras, D. S.; Clancy, Y. L.; Lobkovsky, E. B.; Yaghi, O. M.; Dai, S. *Angew. Chem., Int. Ed.* **2006**, *45*, 1390−1393.
(13) Seo, J. S.; Whang, D.; Lee, H.; Jun, S. I.; Oh, J.; Jeon, Y. J.; Kim, K. *Nature* **2000**, *404*, 982−986.
(14) Wu, C. D.; Hu, A.; Zhang, L.; Lin, W. B. *J. Am. Chem. Soc.* **2005**, *127*, 8940−8941.

(NLO) applications[15] and asymmetric catalysis,[14] for example, and led us to postulate that MOFs could offer predictable, well-defined environments for chromophores in solid-state materials.

Despite the large number of MOF materials described in the literature, however, reports of luminescent MOFs are scarce, especially those that display ligand-based emission.[5,16,17] The majority of materials in this class exhibit metal ion-centered luminescence due to the incorporation of lanthanide elements into their framework.[18–20] One potential advantage for the use of ligand-based emission in MOFs is that it should readily be tunable through variation of the nature of the linker and/or the structure of the framework. Additionally, calculations regarding the electronic structure of prototypical porous 3-D MOFs have suggested that the bandgaps of these materials can be altered by changing the degree of conjugation in the ligand.[21] Such factors may prove important for the practical application of these materials.

In this paper, we describe a ligand-based approach to the synthesis of new luminescent MOF compounds. Zinc-based MOF motifs are used to prepare two new extended structures that differ in dimensionality but feature rigid metal−ligand coordination geometries that provide support for a luminescent linker with an inherent degree of flexibility, *trans*-4,4′-stilbene dicarboxylic acid (LH_2; linker unit L). Stilbene has a range of technologically important uses. For example, it is an important component in solid-state scintillating materials, as its luminescence can be used to discriminate neutron and gamma-ray radiation.[22] Additionally, stilbenes are commonly employed as a backbone motif in organic NLO materials[23–25] and may be considered the fundamental unit of the electro- and photo-luminescent conjugated polymer, poly(*p*-phenylenevinylene) (PPV).[26–28]

Our interest in stilbene-based MOFs is 2-fold: first, stilbenes can undergo a light-induced *trans−cis* isomerization, a nonradiative decay pathway that significantly decreases the photo-luminescence quantum yield (QY).[29] However, the QY can theoretically approach 100% when this mechanism is suppressed. Various efforts have been made to rigidify stilbenes, such as increasing media viscosity,[30] incorporation into zeolite pores,[31] binding to antibodies,[32] or synthetically locking the

ethylene unit into the *trans* configuration by ring closure.[33,34] Incorporation of stilbene as the linker into a MOF lattice could potentially suppress this isomerization by fixing the ligand configuration through rigid coordination, affording a material with increased QY and brightness. Second, the low density and regularity of MOFs allows for well-defined interactions between linkers within the framework and with their environment, which may be investigated spectroscopically by suitable choice of ligand chromophore. Stilbene excimer luminescence has been used for sensitive detection of DNA[35] and antibody binding events.[32] We are, therefore, interested in probing structural- and guest-dependent luminescence of stilbene-based MOF materials as model systems and for their potential sensing capabilities.

It is well-established that different crystal structures can result from the same starting materials under different synthetic conditions.[36,37] For example, the use of $Zn(NO_3)_2 \cdot x H_2O$ and 1,4-benzene dicarboxylic acid can yield a variety of MOF structures by varying reaction conditions. These can differ in connectivity and porosity depending on the nature of the secondary building unit (SBU), forming networks with di- and trinuclear cluster SBUs, and 3-D cubic frameworks with tetranuclear SBUs.[37] With this in mind, we sought to form two different zinc-stilbene MOFs, allowing for the study of their luminescence in both 2-D and 3-D extended structures. We report here the synthesis, structure, and luminescent properties of these MOFs, along with their optical response to the exchange of solvent guest molecules. These results show that coordination to the metal clusters in the frameworks imposes structural rigidity on the stilbene moieties, leading to longer luminescence lifetimes and presumably increased QY; this is similar for both structures although a variation in porosity and interchromophore coupling is observed between the 2-D and 3-D structures. In addition, reversible, guest-dependent luminescence suggests that our approach may allow for the design of high-efficiency chromophore assemblies with optical properties suitable for sensing applications.

Results and Discussion

Structure and Characterization. Yellow, needle-like crystals resulted from solvothermal reaction of $Zn(NO_3)_2 \cdot 6H_2O$ and LH_2 in *N,N*-dimethylformamide (DMF) at 70 °C for 16 h and then 85 °C for 4 h. Their formula and structure were determined *via* single-crystal X-ray diffraction and elemental analysis to be $Zn_3L_3(DMF)_2$, **1**; these were obtained phase-pure, as indicated by powder X-ray diffraction (PXRD). **1** is two-periodic, consisting of hexagonal networks composed of trinuclear $Zn_3(RCO_2)_6$ SBUs connected by the organic *trans*-4,4′-stilbene links (Figure 1a). Figure 1b shows that the SBU contains a linear array of three zinc atoms lying on a 3-fold axis; the central

(15) Evans, O. R.; Lin, W. B. *Acc. Chem. Res.* **2002**, *35*, 511−522.
(16) Lee, E. Y.; Jang, S. Y.; Suh, M. P. *J. Am. Chem. Soc.* **2005**, *127*, 6374−6381.
(17) Wang, X. L.; Chao, Q.; Wang, E. B.; Lin, X.; Su, Z. M.; Hu, C. W. *Angew. Chem., Int. Ed.* **2004**, *43*, 5036−5040.
(18) Chandler, B. D.; Cramb, D. T.; Shimizu, G. K. H. *J. Am. Chem. Soc.* **2006**, *32*, 10403−10412.
(19) de Lill, D. T.; Gunning, N. S.; Cahill, C. L. *Inorg. Chem.* **2005**, *44*, 258−266.
(20) Wang, Z.; Jin, C. M.; Shao, T.; Li, Y. Z.; Zhang, K. L.; Zhang, H. T.; You, X. Z. *Inorg. Chem. Commun.* **2002**, *5*, 642−648.
(21) Civalleri, B.; Napoli, F.; Noel, Y.; Roetti, C.; Dovesi, R. *CrystEngComm* **2006**, *8*, 364−371.
(22) Kaschuck, Y.; Esposito, B. *Nucl. Instrum. Methods Phys. Res.* **2005**, *551*, 420−428.
(23) Zojer, E.; Beljonne, D.; Kogej, T.; Vogel, H.; Marder, S. R.; Perry, J. W.; Bredas, J. L. *J. Chem. Phys.* **2002**, *116*, 3646−3658.
(24) Zhu, L. Y.; Yi, Y. P.; Shuai, Z. G.; Bredas, J. L.; Beljonne, D.; Zojer, E. *J. Chem. Phys.* **2006**, *125*, 044101.
(25) Albota, M. et al. *Science* **1998**, *281*, 1653−1656.
(26) Cornil, J.; dos Santos, D. A.; Crispin, X.; Silbey, R.; Bredas, J. L. *J. Am. Chem. Soc.* **1998**, *120*, 1289−1299.
(27) Cacialli, F.; Chuah, B. S.; Kim, J. S.; dos Santos, D. A.; Friend, R. H.; Moratti, S. C.; Holmes, A. B.; Bredas, J. L. *Synth. Met.* **1999**, *102*, 924−925.
(28) Meier, H. *Angew. Chem., Int. Ed.* **1992**, *31*, 1399−1420.
(29) Saltiel, J. *J. Am. Chem. Soc.* **1967**, *89*, 1036−1037.
(30) Waldeck, D. H. *Chem. Rev.* **1991**, *91*, 415−436.
(31) Ramamurthy, V.; Caspar, J. V.; Corbin, D. R.; Eaton, D. F. *J. Photochem. Photobiol. A* **1990**, *51*, 259−263.

(32) Simeonov, A.; Matsushita, M.; Juban, E. A.; Thompson, E. H. Z.; Hoffman, T. Z.; Beuscher, A. E.; Taylor, M. J.; Wirsching, P.; Rettig, W.; McCusker, J. K.; Stevens, R. C.; Millar, D. P.; Schultz, P. G.; Lerner, R. A.; Janda, K. D. *Science* **2000**, *290*, 307−313.
(33) Oelgemoller, M.; Brem, B.; Frank, R.; Schneider, S.; Lenoir, D.; Hertkorn, N.; Origane, Y.; Lemmen, P.; Lex, J.; Inoue, Y. *J. Chem. Soc., Perkin Trans. 2* **2002**, 1760−1771.
(34) Saltiel, J.; Marinari, A.; Chang, D. W. L.; Mitchener, J. C.; Megarity, E. D. *J. Am. Chem. Soc.* **1979**, *101*, 2982−2996.
(35) Letsinger, R. L.; Wu, T. F. *J. Am. Chem. Soc.* **1995**, *117*, 7323−7328.
(36) Halper, S. R.; Do, L.; Stork, J. R.; Cohen, S. M. *J. Am. Chem. Soc.* **2006**, *128*, 15255−15268.
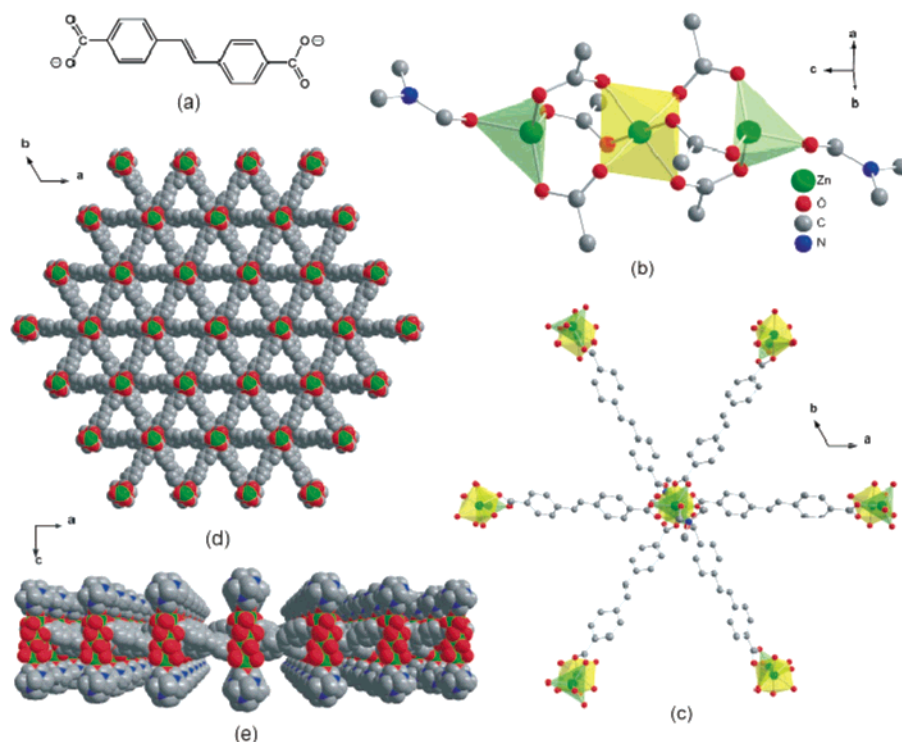(37) Eddaoudi, M.; Li, H. L.; Yaghi, O. M. *J. Am. Chem. Soc.* **2000**, *122*, 1391−1397.

Figure 1. (a) *trans*-4,4′-Stilbenedicarboxylate linker, L. (b) View of X-ray crystal structure of **1** parallel to the *c*-axis, showing $Zn_3(RCO_2)_6(DMF)_2$ SBU along with C(4) atoms of stilbene rings. Only one orientation of disordered DMF is shown; O_h Zn coordination polyhedron is yellow, T_d polyhedra are green. (c) View of **1** looking down onto this SBU, showing the hexagonal pinwheel connections between adjacent SBUs made by the linker units. (d) Space-filling model of **1** looking down *c*, showing the 2-D network formed. (e) Space-filling model of a single layer of **1** looking down *b*, showing terminal T_d Zn atoms capped by disordered DMF molecules above and below the layer, with the Zn-L network extending in the *ab*-plane.

zinc atom rests on a crystallographic inversion center. The overall symmetry of the SBU is S_6, so that the carboxylate groups bridge the zinc atoms in a nonplanar *syn*-skew fashion (*cis*-O−Zn−O angles deviate only slightly from 90°), allowing the stilbene linker to remain planar (torsion angles between phenyl rings <2°). The central zinc atom has octahedral coordination, while the terminal zincs are tetrahedral; their apical sites are occupied by O atoms of monodentate DMF molecules, which themselves exhibit disorder over three possible orientations relative to the 3-fold axis. The Zn−O bonds of the central hexacoordinated zinc atom are evidently longer than those of the tetracoordinated zinc atoms; moreover, the Zn−O(DMF) bond length lies between the Zn−O bond lengths for tetra- and hexacoordinated zinc atoms. The Zn···Zn separation of 3.515 Å does not indicate any significant direct interaction between the metal atoms; this distance is constrained by the bridging geometry.

The SBUs are connected by linker units in a hexagonal pinwheel geometry, affording a 2-D, layered arrangement (Figure 1c and 1d) with disordered DMF filling space above and below the layer units (Figure 1e). Individual layers stack together with a cubic *ABCABC* motif, resulting in a dense structure ($d = 1.52$ g/cm³) without significant overall porosity (i.e., triangular pores visible in Figure 1d are, in fact, partially occupied by the packing of additional layers). **1** is isostructural with a recently reported Co-stilbene MOF, also prepared in DMF.[38]

Variation of the solvothermal synthesis of **1** substituting *N,N*-diethylformamide (DEF) as the solvent at 105 °C for 16 h

(38) Park, G.; Kim, H.; Lee, G. H.; Park, S.-K.; Kim, K. *Bull. Korean Chem. Soc.* **2006**, *27*, 443−446.

afforded colorless, prism-like crystals. Single-crystal XRD reveals these to have a porous 3-D framework structure, **2**, consisting of two interpenetrated networks with formula unit Zn_4OL_3, which exhibit a distorted primitive cubic topology with elementary cage size $a \approx b \approx c \approx 19.4$ Å and $\alpha \approx \beta \approx 90$, $\gamma \approx 77°$ (Figure 2). Growth of these crystals requires temperatures above 100 °C to yield phase-pure materials, otherwise traces of other unidentified phases (possibly including **1**) are observed in the PXRD patterns. However, **2** was never observed by PXRD as a byproduct of the **1** syntheses described above.

Each of the frameworks in the structure of **2** is constructed from basic zinc carboxylate units $Zn_4O(RCO_2)_6$ as the SBUs, which are bridged by the organic *trans*-4,4′-stilbene links. Figure 2a shows this SBU is a cluster with tetrahedral local coordination about each zinc atom; the carboxylate C atoms of each cluster serve as points-of-extension that define the vertices of an octahedron. The stilbene units are essentially planar, if slightly more distorted than in **1** (torsion angles between phenyl rings <5°). Although the positions of the framework atoms were determined accurately, the free guest chloroform and DMF molecules filling the pores were not located due to the highly porous nature of **2** and the disorder problems usually encountered in this type of structure. Despite being interpenetrated, the structure of **2** contains large cavities; in particular, there are 17.1 × 17.1 Å channels in the [010] projection, as shown in Figure 2c. Moreover, in the overall crystal structure of **2,** there exist no specific interactions between the two interpenetrated frameworks, so the maximum internal pore size can be represented as a sphere with diameter 16.5 Å, where this diameter is equal to the distance of separation between the van der Waals surfaces of the frameworks.
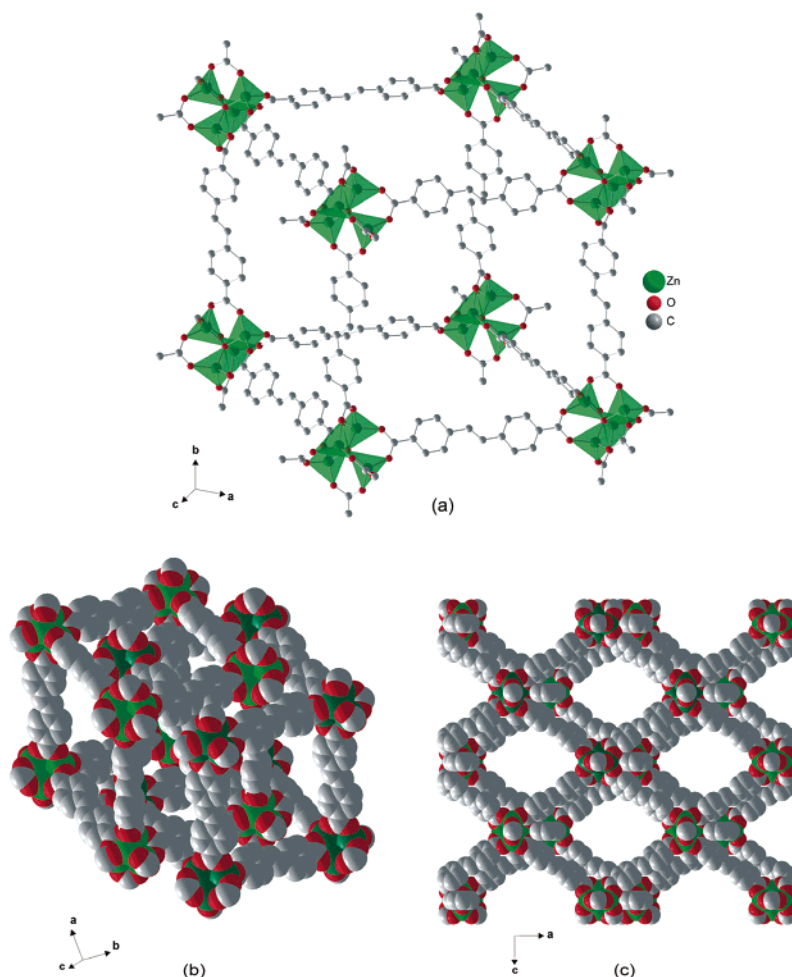
Figure 2. X-ray crystal structure of **2**, showing cubic framework of $Zn_4O(RCO_2)_6$ SBUs connected by *trans*-stilbene linkers and green T_d Zn coordination polyhedra (a), and (b) a space-filling model showing interpenetrated, porous lattice of two distinct cubic nets (light and dark green Zn atoms, respectively). The pores extend through the crystal, as shown for the [010] projection in part c.

This framework structure is analogous to the so-called IRMOF series, all of which are three-periodic, cubic-type structures with $Zn_4O(RCO_2)_6$ SBUs. Interestingly, the synthesis of **2** required conditions similar to those reported by Yaghi and co-workers to favor construction of this particular SBU, a compelling illustration that chemical control may be used to give materials with tunable properties, but similar topologies.[7,39]

Crystals of **1** are air-stable and maintain their structure after evacuation at 100 °C, as determined by PXRD (see Supporting Information) and elemental analysis. Thermogravimetric analysis (TGA) indicates loss of 2 equiv of DMF (~13 wt %) above 250 °C, followed by full decomposition at higher temperature, as shown in Figure 3a. Unfortunately, attempted removal of coordinated DMF from crystals of **1** by evacuation at 250 °C in an effort to generate a structure with unsaturated zinc centers gave substantial decomposition.

Crystals of **2** contain incorporated guest solvent molecules that can be exchanged, although extended evacuation results in an irreversible structural change and significant loss of crystallinity (determined by PXRD, see Supporting Information). Similar behavior has been found previously for a zinc MOF with a comparable, interpenetrated structure (IRMOF-9, linker = 4,4′-biphenyl dicarboxylate); this has been attributed to a
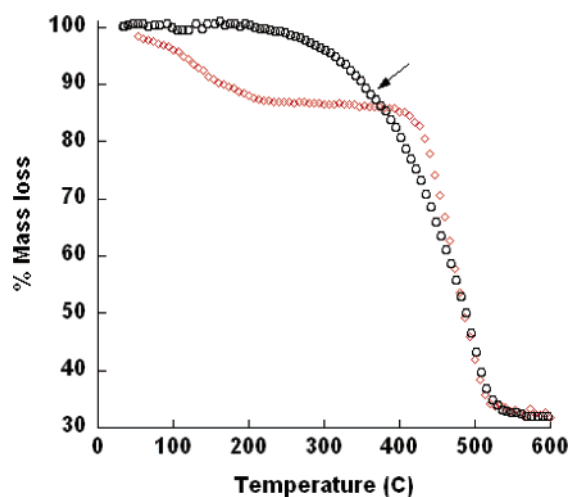
(39) Eddaoudi, M.; Kim, J.; Rosi, N.; Vodak, D.; Wachter, J.; O'Keeffe, M.; Yaghi, O. M. *Science* **2002**, *295*, 469−472.

Figure 3. Thermogravimetric analysis (TGA) data for **1** (black circles) and **2** (red diamonds). For the 2-D MOFs (**1**), mass loss of strongly coordinated DMF occurs (13%, see arrow), followed by steady decomposition which continues until 520 °C. For the 3-D MOFs (**2**), initial mass loss from solvent incorporated into the pores is evident until approximately 200 °C (15%, approximately 1 equiv of DMF and 1 equiv of CHCl₃), followed by a plateau after which a relatively sharp decomposition occurs at 400 °C.

weakening of the interactions between interpenetrated units when the ligand is relatively long and flexible, and the misalignment of these units upon solvent removal.[7] Lumines-
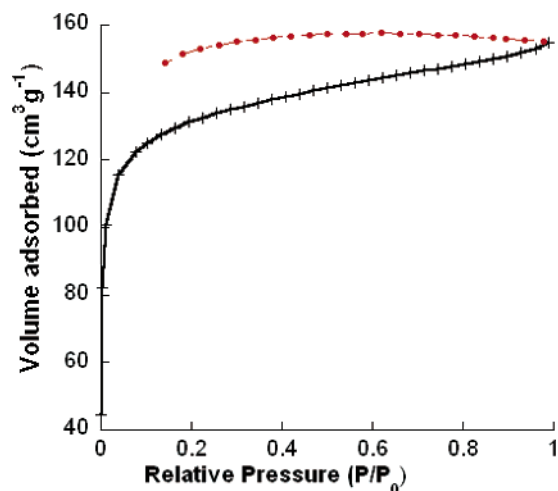
Figure 4. Nitrogen sorption isotherm for **2** measured at 77 K. Adsorption is shown in black hatches, desorption in red circles. Langmuir surface area is estimated to be 580 ± 6 m^2/g.

cence studies for **2** (see below) suggest that, in the solvated structure, no significant interaction occurs between the stilbene units of the interpenetrated frameworks, and, thus, the lack of substantial cohesive forces between these units results in a similar structural collapse after solvent loss. Although interpenetration decreases the pore size compared to a fully open structure, the calculated solvent accessible portion accounts for 76.2% of the crystal volume, with a pore diameter of 16.5 Å and density 0.50 g/cm^3 (respective values for IRMOF-9 are 74.7%, 14.5 Å and 0.66 g/cm^3).[39] TGA data shown in Figure 3b reveal that, after mass loss from incorporated solvent in the pores ($\sim$15 wt %), **2** is thermally stable up to 410 °C before the onset of further mass loss.

Crystals of **1** display no significant surface area through gas sorption measurements, as expected due to their high density and the pore occlusion evident in their crystal structure. In contrast, surface area measurements for **2** exhibit a Type I sorption isotherm (indicative of homogeneous micropores) with a Langmuir surface area of 580 m^2/g. This value is lower than typical for comparable MOF structures (commonly 1000−4300 m^2/g)[7,39] presumably due to the structural change upon evacuation resulting in a partial collapse of the framework; however, this indicates that the evacuated structure still retains some porosity. The adsorption/desorption profile displays significant hysteresis (see Figure 4), suggesting that there may also be a structural alteration during measurement, possibly due to a change in interaction between the catenated units and/or the linker exhibiting flexibility (e.g., about the double bond) under these conditions. Recently, MOFs containing a similar linker (*trans*-4,4′-bis(4-pyridyl)ethene) have been shown to display anomalous sorption behavior due to dynamic shape changes, which can also be induced by variation of incorporated guest molecules.[40] Dynamic structural changes in the framework may be desirable for advanced applications, such as combined sensing and separation. For example, MOFs with similar interpenetrated structures have been reported to undergo structural changes that allow for size- and shape-matching of guests and their use in GC separations of alkanes.[12]
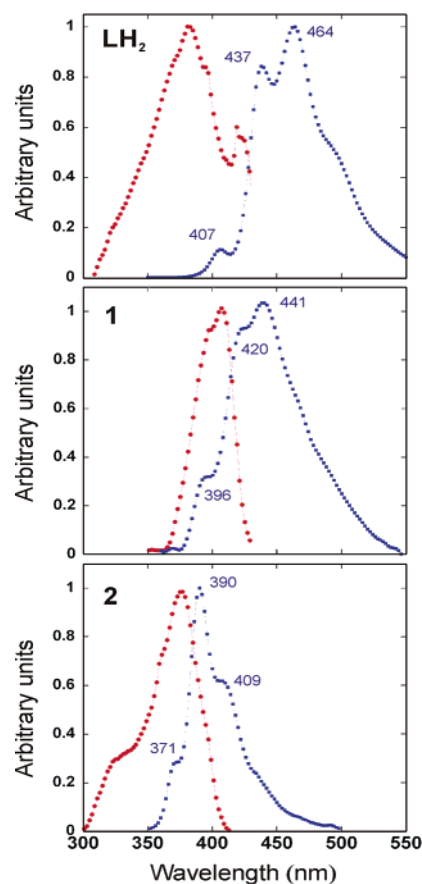
(40) Chen, B.; Ma, S.; Zapata, F.; Lobkovsky, E. B.; Yang, J. *Inorg. Chem.* **2006**, *45*, 5718−5720.

Figure 5. Normalized excitation (red circles) and emission (blue squares) spectra for LH$_2$ (as a powder sample, top), **1** (middle), and **2** (bottom). Spectra of **1** and **2** were obtained for individual crystals soaked in CHCl$_3$. $\lambda_{ex} = 350$ nm for LH$_2$ and **1**, 325 nm for **2**. Emission maxima for the first three vibronic bands are indicated. Excitation spectra were detected at 450 nm.

Photoluminescence Studies. Crystals of **1** and **2** contain the same linker in two different, well-defined geometries, allowing for a comparative study of their photoluminescence and its interpretation with regard to the local linker environment within each structure. Both appear very bright to the eye upon illumination with UV light but differ in color. Crystals of **1** are yellow in color and produce blue emission, while crystals of **2** are colorless, with purple/blue emission, consistent with their structural differences as outlined below. Figure 5 shows combined excitation/emission spectra of crystalline **1** and **2** soaked in chloroform, compared to a powder sample of *trans*-4,4′-stilbene dicarboxylic acid (LH$_2$) precursor. The emission spectrum of **2** in the solid is nearly identical in position to dilute solutions of LH$_2$ in DMSO/H$_2$O (100:1 v/v) (see Supporting Information), suggesting little contribution from the Zn$_4$O clusters to the emission; the red-shift observed for these species compared to *trans*-stilbene itself[30] is consistent with the small increase in conjugation due to the carboxylate units.

The differences observed in the electronic spectra for **1** and **2** likely have their origins in a number of factors, including the local coordination environment of the ligand and the steric proximity of ligands to each other and to other species present in the unit cell. The zinc cluster types in **1** and **2** may potentially exert disparate influences on the local electronic structure of the linker unit (for example, the clusters may differ in Lewis acidity). However, studies of related MOFs suggest that the

direct electronic influence of this cluster type is likely to be small. The excitation spectrum of IRMOF-1 is reported to be very similar to that of powdered 1,4-benzene dicarboxylic acid disodium salt; that is, the Zn_4O clusters in the framework do not perturb the electronic structure of the linker significantly.[41] Theoretical studies of this MOF indicate that the highest occupied valence levels are dominated by *p*-orbitals of the aromatic carbon atoms with a small contribution from the carboxylate atoms;[21] additionally, related studies suggest that the band gap in IRMOF-1 remains unchanged when the Zn atom is replaced by Be, Mg, Ca, or Cd.[42] Very recently, 2-D cadmium MOFs containing the fluorophore 5-sulfosalicylic acid (SSA) were found to display intense ligand-based emission with a small red-shift observed between solid samples of the free ligand and the complex (388 nm vs 394 nm); DFT MO calculations suggest that this bathochromic shift is due to deprotonation of H_3SSA and not coordination to Cd^{2+}.[43] We have found that the differences observed between dilute solutions of LH_2 and its disodium salt (8 nm red-shift in emission for Na_2L, see Supporting Information) are small in comparison to the differences observed between the electronic spectra of **1** and **2** (≥ 30 nm difference in emission).

Furthermore, two 2-D zinc MOFs based on norfloxacin are reported to exhibit ligand-based emission; they have similar coordination environments (both octahedral Zn^{2+} bound to two carboxylate ligands), but a significant blue-shift in emission (420 nm vs 440 nm) is observed for the lower-density structure compared to the higher-density material and the powdered ligand (both of which display very similar emission). These differences are attributed to a decrease in interligand $\pi-\pi$ interactions in the lower density structure.[44] Therefore, we believe the differences between spectra of **1** and **2** are likely a result of crystal density, as the evidence indicates that the influence of the different types of zinc cluster on the electronic spectra observed is small compared to that of the differences in interchromophore interaction within each structure. This is supported by time-resolved studies described in detail below.

Crystals of **1** and **2** both show structured emission bands similar to that for LH_2 in the solid state (Figure 5) and in solution, with several vibronic bands evident. This supports our interpretation that emission is essentially ligand-based, with little contribution from the metal cluster units in the framework. The behavior observed for **2** differs from that described in the literature for IRMOF-1, for which a green luminescence is attributed to energy transfer from the relatively nonfluorescent linker (1,4-benzenedicarboxylate) to the Zn_4O units.[41] The emission spectrum of **2** is similar in structure to *trans*-stilbene in dilute solution[1] and in the crystalline state[45] (which has a herringbone packing structure),[46] although for both **1** and **2** the vibronic structure is more pronounced at room temperature. This indicates that the stilbene units are rigidified in **1** and **2**; indeed, this structure resembles that for synthetically locked stilbene

derivatives,[33] as discussed in more detail below. The local site symmetry of the ligand in each structure is likely to have a significant influence on the relative intensities of the vibronic bands evident;[47] however a detailed interpretation of the differences observed between **1** and **2** in this context is beyond the scope of the current study. We note, however, that the relative ratios of the vibronic peaks were found to vary between samples of **1** yet remained nearly identical among many different crystals of **2**.

The fine structure displayed in solid-state electronic spectra of conjugated organic molecules has received a great deal of attention, as analysis can reveal information about the interactions between chromophore units and chromophore rigidity, along with variations in the environmental geometry.[33,48] The intensity of the lowest energy emission peak (0−0) is sensitive to the degree of interchromophore coupling, decreasing significantly upon chromophore aggregation. Cofacial arrangements ≤ 4 Å apart typically show strong intermolecular coupling *via* $\pi-\pi$ overlap,[26] resulting in substantial loss of electronic fine structure. Non-cofacial chromophore assemblies and/or those further apart in space (ca. 4 Å to 8 Å) can show an intermediate degree of coupling, the details of which depend significantly on the geometry of the arrangement. Trap emission in solid PPV films has been attributed to the creation of stilbenoid dimers, which form excimers that give a red-shifted, structureless emission band with a radiative lifetime significantly longer than for the individual chromophore.[1] The vibronic structure in the emission spectra of both **1** and **2** is well resolved, so a large contribution of excimer emission to the spectra of both crystals can be ruled out. Neither **1** nor **2** have short cofacial chromophore distances in their crystal structures. The nearest-neighbor distances between aromatic ring centroids and the angles between ring planes are 5.6 Å, 79° (**1**, in an individual layer), 6.0 Å, 0° (**1**, between adjacent layers), and 5.6 Å, 49° (**2**, between interpenetrated cubes along the edge defined by the *b*-axis).

Crystals of **1** show a red-shift and broadening in emission compared to **2**, indicating a greater degree of interchromophore coupling in the 2-D MOF structure, presumably a consequence of the 6.0 Å distance between chromophores in the displaced face-to-face stacking of successive layers. However, the extent of this chromophore interaction in **1** is small compared to LH_2, which displays a significantly red-shifted and broadened emission spectrum. Here, presumably, hydrogen bonding between terminal carboxylic acid groups introduces short interchromophore stacking distances, as observed for *trans*-4,4′-stilbene diamides[49] which show emission spectra characteristic of edge-to-face dimers[50] (5.0 Å between phenyl ring centroids, 28° between ring planes). As described above, the emission spectrum of **2** is very similar to that of LH_2 in dilute solution, indicating these units interact only weakly with one another in this low-density 3-D MOF environment.

The differences between excitation and emission peak maxima for both **1** and **2** are significantly smaller than for dilute

(41) Bordiga, S.; Lamberti, C.; Ricchiardi, G.; Regli, L.; Bonino, F.; Damin, A.; Lillerud, K.-P.; Bjorgenb, M.; Zecchina, A. *Chem. Commun.* **2004**, 2300−2301.
(42) Fuentes-Cabrera, M.; Nicholson, D. M.; Sumpter, B. G.; Widom, M. *J. Chem. Phys.* **2005**, *123*, 124713.
(43) Lu, Z.; Wen, L.; Ni, Z.; Li, Y.; Zhu, H.; Meng, Q. *Cryst. Growth Des.* **2007**, *7*, 268−274.
(44) Chen, Z.-F.; Xiong, R.-G.; Zhang, J.; Chen, X.-T.; Xue, Z.-L.; You, X.-Z. *Inorg. Chem.* **2001**, *40*, 4075−4077.
(45) Gudipati, M. S. *J. Phys. Chem.* **1993**, *97*, 8602−8607.
(46) Hoekstra, A.; Meertens, P.; Vos, A. *Acta Crystallogr. B* **1975**, *31*, 2813−2817.
(47) Pope, M.; Swenberg, C. E. *Electronic Processes in Organic Crystals and Polymers*; 2nd ed.; Oxford Science Publications: New York, 1999.
(48) Spano, F. C. *Ann. Rev. Phys. Chem.* **2006**, *57*, 217−243.
(49) Lewis, F. D.; Yang, J. S.; Stern, C. L. *J. Am. Chem. Soc.* **1996**, *118*, 12029−12037.
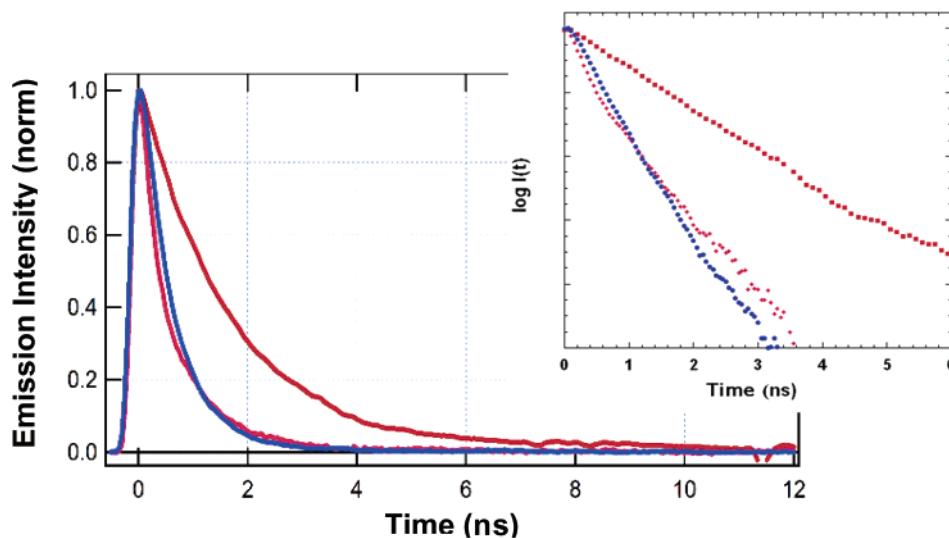(50) Lewis, F. D.; Yang, J. S.; Stern, C. L. *J. Am. Chem. Soc.* **1996**, *118*, 2772−2773.

Figure 6. Emission decays (left) of **1** (pink), **2** (blue), and LH$_2$ (red), and semilogarithmic emission decay plots (right). All three were detected at their respective third vibronic peak (see Figure 5). Emission lifetimes (τ) were determined by fitting the decays to a single or double exponential function: $I(t) = \alpha_1 e^{-t/\tau_1} + \alpha_2 e^{-t/\tau_2}$, where α is the pre-exponential factor, and t is the time. Both **1** and LH$_2$ were best fit to biexponentials, as supported by the semilogarithmic plots (inset) where the presence of more than one decay process with characteristic lifetime results in curvature of these spectra; $\tau_1 = 0.20$ ns, $\tau_2 = 0.95$ ns, $\alpha_1/\alpha_2 = 5.0$ for **1** and $\tau_1 = 0.73$ ns, $\tau_2 = 2.49$ ns, $\alpha_1/\alpha_2 = 1.8$ for LH$_2$ In comparison, **2** was best fit to a monoexponential decay $\tau_1 = 0.50$ ns, resulting in a linear semilogarithmic plot.

solutions of *trans*-stilbene ($\sim$3400 cm^{-1} in dioxane)[1] and LH$_2$ (4088 cm^{-1} in DMSO/H$_2$O (100:1 v/v)), and this difference is smaller for **2** (815 cm^{-1}) than for **1** (1215 cm^{-1}). These data indicate the degree of reorganization between the ground and first excited states of **1** and **2** is reduced compared to *trans*-stilbene and LH$_2$ in solution, reflecting the increased rigidity of the stilbenoid unit afforded through strong coordination by the metal ions in the framework, which results in a larger barrier for torsion about the central ethylene bond.

Time-resolved emission measurements were used to probe further the local environment of stilbenoid units in crystals of **1** and **2**, and emission decay curves are shown in Figure 6. The radiative lifetime of *trans*-stilbene (τ) is estimated to be 1.7 ns,[51] which typically becomes shortened to $\tau < 100$ ps in solution at room temperature. The major factor contributing to the reduced lifetime is the *trans*–*cis* isomerization.[30] These isomers are nearly isoenergetic in the ground state, but a large barrier to rotation exists and the *trans* state acts as a quantum well. Excitation to the first excited-singlet state is followed by barrierless rotation about the central double bond, leading to the essentially nonfluorescent *cis* isomer,[29,32] which can give additional photoproducts, including cyclization to dihydrophenanthrene. This photoisomerization QY is significantly larger than the fluorescence quantum yield at room temperature ($\theta_{PI} = 0.45$ vs $\theta_{EM} = 0.02$ in acetonitrile).[52]

Emission decays for **1** were fit best by a biexponential function. The faster component has $\tau = 0.20$ ns, likely due to emission from monomeric stilbenoid units. The relative contribution of the longer-lived species, with a lifetime of 0.95 ns, was found to increase upon increasing the detection wavelength, along with a concomitant delay observed in the decay curve (see Supporting Information for wavelength-dependent data). Growth of a decay component with longer lifetime at lower emission energy, along with a delay in emission, is indicative

of an excited-state process (i.e., population of the long-lived emissive state occurs after initial excitation), presumably facilitated by interactions between individual chromophores in **1**.[53] Consistent with this, LH$_2$ powder samples show significantly more pronounced behavior in this regard due to much stronger interchromophore coupling. The steady-state emission spectra of **1** remain unchanged upon variation of the excitation wavelength across the full excitation spectrum, indicating there is likely to be only one species contributing to the emission,[54] supporting the assignment of these differences in the time-resolved spectra to an excited-state activated process. In addition, the time-resolved data were found to be reproducible between different crystal samples. These considerations allow us to discount significant influence of sample heterogeneity upon the measurements. The behavior exhibited by **1** is consistent with that found by Bazan and co-workers for paracyclophane-based stilbenoid dimers, which exhibit biexponential emission decays in solution, presumably from different electronic states localized on the monomer and dimer.[2] The longer emission lifetime of **1** is of the order of those found for stilbenoid dimers in the intermediate coupling regime.[50] No changes in the time-resolved spectra for **1** are found between samples immersed in chloroform and those dried *in vacuo*.

In contrast, emission decays for **2** (in a chloroform environment) were best fit by a monoexponential function with $\tau = 0.50$ ns, attributed to emission from stilbenoid monomers. The measured lifetime is approximately five times greater than for *trans*-stilbene in solution, consistent with an increased rigidity of coordinated stilbenoid chromophores in **2**. Typically, increased lifetimes accompany an increase in emission QYs, provided that the radiative decay rate does not change,[55] and therefore the QY of both **1** and **2** may be expected to be larger than for *trans*-stilbene in solution. However, values were not

(51) Syage, J. A.; Lambert, W. R.; Felker, P. M.; Zewail, A. H.; Hochstrasser, R. M. *Chem. Phys. Lett.* **1982**, *88*, 266–270.
(52) Mazzucato, U. *Pure Appl. Chem.* **1982**, *54*, 1705–1721.

(53) Song, Q.; Bohn, P. W.; Blanchard, G. J. *J. Phys. Chem. B* **1997**, *101*, 8865–8873.
(54) Haas, E.; Fischer, G.; Fischer, E. *J. Phys. Chem.* **1978**, *82*, 1638–1643.
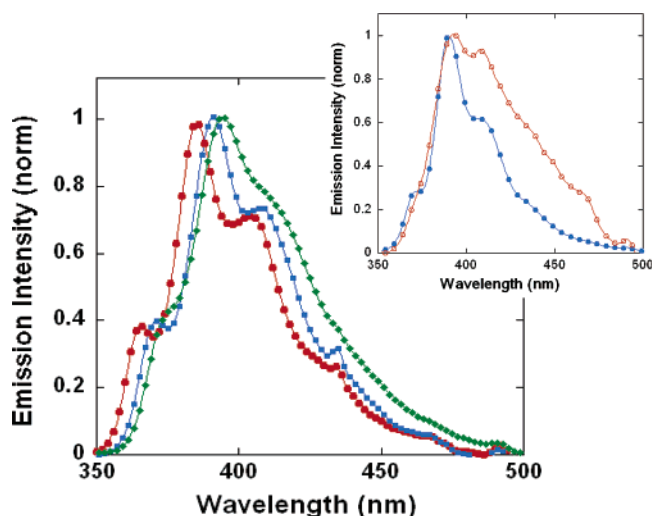(55) Lakowicz, J. R. *Principles of Fluorescence Spectroscopy*; 2nd ed.; Plenum US: New York, 1999.

Figure 7. Solvent-dependent, normalized emission spectra from a crystal of **2** soaked in toluene (green diamonds), chloroform (blue squares), and hexane (red circles). These are fully reversible upon solvent exchange. The inset shows crystals of **2** in chloroform (blue closed circles) and crystals after extended evacuation, under nitrogen (orange open circles). The original spectrum cannot be fully regenerated upon rewetting in chloroform because of a partial structural collapse in the crystal upon evacuation.

determined in this study as variations in crystal size and shape can introduce significant uncertainties into the measurements.

An increase in the luminescence lifetime for **2** may be expected when considering the strong coordination to the Zn_4O units in the crystals. However, this lifetime is shorter than that of "chemically" frozen stilbenes and those highly rigidified in solid matrices shown previously,[56] indicating that the structure is not completely rigid, and thus nonradiative decay pathways are not fully suppressed. We and others have recently addressed the flexibility of MOF-type structures by theoretical means. Molecular dynamics simulations using a newly developed nonrigid force-field indicate that there is considerable motion of the linker groups in IRMOF-1 ($Zn_4O(1,4$-benzenedicarboxylate)$_3$) at room temperature.[57] In addition, Mattesini et al. have used plane-wave density function theory to predict the elastic properties of IRMOF-1 and concluded that, contrary to what was originally thought for this archetypal isoreticular structure, IRMOF-1 is actually *not* an exceptionally rigid material. Instead, the calculations predict it to be a soft and ductile material, with a Young's modulus of 14.8 GPa.[58] Most recently, it was shown that lattice motions need be included to accurately simulate molecular transport in IRMOF-1.[59] By analogy with these results, the porous stilbene-containing structure of **2** (with a longer and less-rigid ligand than IRMOF-1) is expected to provide an environment with increased rigidity and site isolation of ligands, yet flexibility for active interaction with guests incorporated into the open framework.

To investigate the effects of guest molecule incorporation, the emission spectra of **1** and **2** were recorded after exposure to different solvents. Crystals of **1** exhibit no change in emission upon changing solvent environment, and likewise show no

significant difference after drying for extended periods under vacuum. This is likely a function of the dense, rigid structure of **1**, wherein the majority of chromophores are not exposed to the solvent. In contrast, the luminescence from crystals of **2** is sensitive to solvent exchange. Shifts in emission were observed upon changing the solvent, with peak maxima decreasing in energy in the order hexane > chloroform > toluene, alongside a concurrent broadening of the vibronic structure (Figure 7). This response was found to be fully reversible through multiple cycles of exchanges between the different solvents. However, upon complete removal of incorporated solvent *in vacuo*, crystals of **2** display a significant, irreversible red-shift in emission, indicating increased interligand coupling, as shown in the inset of Figure 7. This behavior is ascribable to a permanent structural change which brings the stilbenoid linker units in closer proximity to one another and provides evidence for the hypothesized structural collapse of interpenetrated units upon evacuation, resulting in the lower-than-expected surface areas discussed previously. These results also suggest that the dynamic nature of the lattice of **2** could allow for specific guest–host interactions with this linker, which may have potential application in combined separation and detection experiments.

Summary

We have prepared two luminescent stilbene-based MOFs in which the organic linker serves as the chromophore. The structure of the materials obtained is a function of the synthetic conditions employed. Single-crystal XRD and electronic spectroscopy were used to investigate the local environments of the stibenoid units in the frameworks. In both cases, the ligand becomes rigidified in the *trans* geometry upon coordination to the metal. In the dense, 2-D layered structure, **1**, the chromophore environment allows for a limited degree of ligand–ligand interaction. The porous 3-D cubic framework, **2**, exhibits less significant interchromophore interaction, and the stilbenoid units maintain a degree of flexibility for dynamic interactions with guests. Initial studies reveal that crystals of **2** show reversible, guest solvent-dependent emission. Sensing with an inherently luminescent MOF with the potential to undergo dynamic shape changes with specific guests is an exciting possibility that we hope to explore in future separations-based experiments.

Experimental Section

Synthesis. 4,4′-Stilbenedicarboxylic acid (LH$_2$) and *N,N*-dimethylformamide (DMF) were purchased from Alfa Aesar. $Zn(NO_3)_2 \cdot 6H_2O$ and chloroform (CHCl$_3$) were purchased from Fluka. *N,N*-Diethylformamide (DEF) was purchased from TCI America.

1: A 71.3 mg amount of LH$_2$ was added to 20 mL of DMF in a Pyrex glass jar and agitated until almost fully dissolved. To this was added 209.2 mg of $Zn(NO_3)_2 \cdot 6H_2O$ (3:1 mole ratio of metal to linker). This was sealed and placed in an oven at 75 °C for 16 h, followed by 85 °C for 4 h, yielding transparent yellow crystals of **1**. These were collected and washed three times with fresh DMF and three times with chloroform, dried at 65 °C in vacuo for 6 h, and then stored under ambient conditions. Yield: 75.2 mg (74% based on LH$_2$). Analysis calcd (%) for $Zn_3L_3(DMF)_2$: C 56.83, H 3.89, N 2.45; found: C 56.61, H 4.39, N 2.88. IR (KBr, cm^{-1}): 3424 (br, w), 3060 (w), 2998 (w), 2927 (w), 1660 (s), 1607 (s), 1544 (s), 1394 (br), 1182 (m), 1109 (m), 1056 (w), 1014 (m), 979 (m), 906 (m), 867 (m), 856 (m), 805 (m), 793 (s), 714 (s), 684 (m), 644 (s), 569 (m), 524 (m), 473 (w). Solid-

(56) Pyun, C.-H.; Lyle, T. A.; Daub, G. H.; Park, M. *Chem. Phys. Lett.* **1986**, *124*, 48−52.
(57) Greathouse, J. A.; Allendorf, M. D. *J. Am. Chem. Soc.* **2006**, *128*, 10678−10679.
(58) Mattesini, M.; Soler, J. M.; Yndurain, F. *Phys. Rev. B* **2006**, *73*, 094111.
(59) Amirjalayer, S.; Tafipolsky, M.; Schmid, R. *Angew. Chem., Int. Ed.* **2007**, *46*, 463−466.

state UV/vis (KBr, λ_{max}): 366 nm, 336 nm. TGA indicates loss of coordinated solvent beginning at 250 °C, followed by full decomposition.

2: A 30.7 mg amount of LH_2 was added to 20 mL of DEF in a Pyrex glass jar and sonicated upon light heating to enable its suspension. A 209.2 mg amount of $Zn(NO_3)_2 \cdot 6H_2O$ was added and the jar sealed (6:1 mole ratio of metal to linker). This was placed in an oven at 105 °C for 16 h, yielding transparent colorless crystals of **2**. DEF was decanted while still hot and replaced by DMF. Crystals of **2** were washed with chloroform three times and stored in chloroform until ready for use. Yield 33.8 mg (70% based on LH_2). Analysis calcd (%) for $Zn_4OL_3(DMF)(CHCl_3)$: C 49.20, H 3.03, N 1.10; found: C 49.70, H 3.24, N 1.08. IR (KBr, cm^{-1}): 3455 (br), 3024 (w), 3008 (w), 1606 (s), 1540 (s), 1395 (br), 1180 (s), 1102 (m), 1014 (m), 953 (w), 858 (m), 784 (s), 751 (m), 708 (s), 671 (w), 646 (m), 569 (w). Solid-state UV/vis (KBr, λ_{max}): 378 nm, 334 nm. TGA indicates continuous loss of adsorbed solvent until 200 °C and sharp decomposition at 410 °C.

Physical Characterization. TGA was performed on a Pyrus II Perkin-Elmer under He. Surface areas were measured on a Micromiretics ASAP 2000 Porosimeter with N_2 as the sorption gas. Powder XRD was performed on a Scintag X'Pert with Cu Kα radiation. Steady-state emission spectra of solid samples were collected with a SPEX Fluoromax using a fiber optic extension.

Single-Crystal Diffraction. Data were collected on a Bruker three-circle diffractometer equipped with a SMART APEX-II CCD area detector with graphite-monochromated Mo Kα radiation ($\lambda = 0.71073$ Å, $2\theta = 52°$). $Zn_3L_3(DMF)_2$, **1**, $C_{54}H_{44}N_2O_{14}Zn_3$, $M_r = 1141.02$, rhombohedral, space group $R\bar{3}$, at $T = 100.0(2)$ K: $a = 16.1661(4)$, $c = 16.4796(9)$ Å, $V = 3729.82(19)$ Å^3, $Z = 3$, $d_{calcd} = 1.524$ g/cm^3, $F(000) = 1752$, $\mu = 1.506$ mm^{-1}. The structure was solved by direct methods and refined by full-matrix least-squares refinement with anisotropic displacement parameters for all non-hydrogen atoms. Two coordinated monodentate DMF ligands are disordered over three sites relative to the 3-fold axis. The hydrogen atoms were generated geometrically and included in the refinement with fixed position and thermal parameters. Final R-factors were $R_1 = 0.0242$ for 1239 reflections with $I \geq 2\sigma(I)$ and $wR_2 = 0.0586$ for all 1480 ($R_{int} = 0.035$) independent reflections. The maximum and minimum peaks on the final difference Fourier map corresponded to 0.258 and -0.307 e/Å^3, respectively. All calculations were carried out using the SHELXTL (PC Version 6.12) program. Zn_4OL_3, **2**, $C_{48}H_{30}O_{13}Zn_4$, $M_r = 1076.2$, orthorhombic, space group $Pnnm$, at $T = 100.0(2)$ K: $a = 30.317$-(12), $b = 19.411(8)$, $c = 24.161(9)$ Å, $V = 14218(10)$ Å^3, $Z = 4$, $d_{calc} = 0.503$ g/cm^3, $F(000) = 2168$, $\mu = 0.687$ mm^{-1}. Refinement of 151 parameters on 5100 independent reflections out of 62286 measured reflections ($R_{int} = 0.1229$) led to $R_1 = 0.0656$ ($I > 2\sigma(I)$), $wR_2 = 0.1662$ (all data), $S = 1.001$. The maximum and minimum peaks on the final difference Fourier map corresponded to 0.564 and -0.447 e/Å^3, respectively. All calculations were carried out using the SHELXTL (PC Version 6.12) program. Contribution from disordered guest molecules was accounted for using the SQUEEZE subroutine within the PLATON software package. Statistics prior to treatment of data with SQUEEZE were $R_1 = 0.1325$ ($I > 2\sigma(I)$), $wR_2 = 0.3866$ (all data) and $S = 1.459$. Calculation of the total solvent-accessible volume was performed using the CALC SOLV routine within the PLATON software package.

Emission Lifetimes. A mode-locked Nd:YAG laser was regeneratively amplified and frequency tripled to produce nearly transform-limited 355 nm pulses. The repetition rate was 20 Hz. The pulse width of the frequency-tripled output of the regeneration is estimated to be approximately 60 ps (fwhm). The 355 nm pulses were focused onto the sample. Emission was collected with an f/4 visible achromat and imaged 1:1 with a second achromat onto the 200 mm wide entrance slit of a 1/8 m monochromator. A 600 lines mm^{-1} grating (blazed for 300 nm) dispersed the emission. The 1200 μm wide exit slit width produced a nearly rectangular bandpass of 7.5 nm. The grating was tuned to collect emission from individual vibronic bands (based on fluorimeter measurements). The filtered emission was detected with a microchannel plate photomultiplier tube (MCP−PMT), and the resulting signal was digitized with a real-time digital oscilloscope and with an analog bandwidth of 6 GHz. The rise time of the detection system is $\sim$150 ps, the fall time is $\sim$300 ps, and the fwhm is $\sim$300 ps. A convolve-and-compare algorithm was used to fit the data with a two-component exponential decay including convolution with the instrument response function, which was recorded by measuring the elastically scattered 355-nm light from the sample substrate. The slight impedance mismatch between the detector, cabling, and oscilloscope produces minor postpulse ringing (<0.5%), which necessitates convolution in the fitting procedure for accurate determination of decay rates.

Supporting Information Available: Crystallographic information files (CIF) for **1** and **2**, PXRD patterns of evacuated crystals, wavelength-dependent emission lifetime data, absorption and emission of LH_2 and Na_2L in DMSO/H_2O (100:1 v/v), and complete reference 25. This material is available free of charge via the Internet at http://pubs.acs.org.

JA0700395